Available online at www.sciencedirect.com
SCIENCE DIRECT®
Journal of Nuclear Materials 327 (2004) 97–113
journal of nuclear materials
www.elsevier.com/locate/jnucmat

A metallographic and fractographic study of outside-in cracking caused by power ramp tests

S. Shimada [a,*], E. Etoh [a], H. Hayashi [b], Y. Tukuta [b]

[a] Global Nuclear Fuel Japan Co., Ltd., 2163, Narita-cho, Oarai-machi, Higashi Ibaraki-gun, Ibaraki-ken 311-1313, Japan
[b] Japan Nuclear Energy Safety Organization, 17-1, 3-chome Toranomon, Minato-ku, Tokyo 105-0001, Japan

Received 24 December 2002; accepted 26 January 2004

Abstract

The failure mechanism experienced by high burnup segment rods in power ramp tests was studied using metallographic and fractographic observations on rods which had been ramp-tested after four and five cycles of base-irradiation in a BWR. The observations revealed that cracking was initiated outside the cladding tubes and penetrated inwards. The process started an axial split with cracking of radial hydrides that were formed during the power ramp test, followed by propagation caused by step-by-step cracking of hydrides at a crack tip. The metallographic observation showed high hydride content in the Zr-layer facing pellet–pellet interfaces. This high hydride content seemed important for the formation of radial hydrides outside the tubes. Hydrogen at the crack tip in the propagation process was produced by oxidation of the crack surface by diffused water vapor and might also be critical to the mechanism as well as hydrogen in the cladding tubes.

PACS: 28.41.Bm; 62.20.Mk

1. Introduction

Zirconium (Zr)-lined Zircaloy-2 cladding tubes have excellent PCI (pellet cladding interaction)-resistance and are generally used as fuel cladding material in BWRs (boiling water reactors). The PCI-resistance of the cladding is widely demonstrated through many power ramp tests up to about 50 GWd/t [1,2]. In the 'High Burnup LUA Program for BWRs' in Japan, Zr-lined cladding was used and some segment rods were power ramp-tested after three, four and five cycles of base-irradiation in a commercial BWR [8,17]. The ramp tests exhibited high performance for the rods irradiated to five cycles, or about to 60 GWd/t. Among five segment rods which failed in the ramp tests, one segment rod after four cycles of irradiation and three segment rods after five cycles of irradiation revealed axial cracks or 'splits' on the outer surfaces. The failed segment after three cycles of irradiation exhibited a pinhole that was typical of PCI/SCC (stress corrosion cracking) failure [3]. The splits were visually similar to the cracks observed on fuel degradation in BWRs except for their length [4–7,18]. Degradation splits have usually been long, sometimes more than 1 m, however, the split length on the failed segment rods was short and ranged from 4 to 40 mm depending on the ramp test conditions. In any cases, the visual appearances of the failed segment rods after four and five exposure cycles suggested that the segment rods failed, not by the usual PCI/SCC, but by a different mechanism. Detailed post irradiation examinations (PIEs) were conducted to observe the outer and inner surfaces of the cladding tubes, fracture surfaces and hydride behavior in the tubes

* Corresponding author. Tel.: +81-29 267 9012; fax: +81-29 267 9014.
E-mail address: sachio.shimada@gnf.com (S. Shimada).

0022-3115/$ - see front matter © 2004 Elsevier B.V. All rights reserved.
doi:10.1016/j.jnucmat.2004.01.022

around through-wall cracks. Full-length rods that experienced only base-irradiation were also examined to compare the hydride behavior with that of ramp-tested segment rods. The metallographic and fractographic observations were used to propose a comprehensive mechanism that dominated the behavior of rods that failed by power ramp tests after four and five cycles of base-irradiation.

2. Experimental

Among 25 segment rods that were subjected to power ramp tests in the Japan Material Test Reactor (JMTR), failure occurred for one rod (P1; D3/F3-3) which had experienced three cycles of base-irradiation, one rod (P2; D4/F3-5) with four cycles, and three rods (P3; D8/C6-5, P4; D8/F3-5 and P5; D8/C6-6) with five cycles. The ramp sequences included a stair case ramp mode and a single step mode [8]. The exposure and ramp test data are summarized in Table 1. The rods ramp-tested after three and four exposure cycles failed in the single mode tests. As for the rods with five cycles, two rods (P3 and P4) failed in the single mode tests and one (P5), in the stair mode. Photos showing outer surfaces of the failed rods are given in Fig. 1. The P1 rod with three exposure cycles showed a small pinhole, while rather long axial cracks were clearly visible on all other rods, P2, P3, P4 and P5, with respective crack lengths of about 4, 5, 10 and 40 mm.

The rods with splits on outer surfaces, P2, P3, P4 and P5, were carefully inspected with emphasis placed on hydride distributions in cladding tubes and fracture surface characteristics. An ordinary inspection was also made for P1 rod which failed by PCI/SCC. Metallographic transverse views and a SEM image of inner surface of P1 are given in Fig. 2 and they reveal a typical PCI/SCC failure mode. As for the rods that failed with splits, periscopic, metallographic and fractographic observations were made for the PIE schemes designated in Fig. 3.

3. Results

3.1. Periscopic observation

Fracture surfaces of P2, P3 and P4 segment rods were observed with a periscope to see the overall fracture surfaces and assess how damaged they were. Fig. 4 is a fracture surface pair for the P2 segment rod. The surfaces were rather clear and bluish, suggesting they were not heavily oxidized. The photos revealed that the fracture surface outline was similar to a semi-ellipse with the long axis on the outside surface. This outline shape indicated that the crack initiated outside and propagated into inwards. Furthermore, many stripe patterns that had similar outlines on the fracture surface were visible there. These patterns suggested that cracks might gradually proceed step-by-step, keeping a fair amount of similarity in the outline shape of the fracture surface.

3.2. Metallographic observation

The hydride distributions around penetrated cracks in P2, P3 and P4 segment rods are given in Fig. 5. These photographs are from specimens mounted transverse to the tube axis. Tiny hydride platelets were distributed only at the outside portion of P2 specimen (Fig. 5(a)), which meant that hydrogen in the tube precipitated only in a narrow band near the outside and was in solution in the remaining areas during the ramp test. Fig. 5(a) illustrates the predominant circumferential orientation of the hydrides in the band, but some radial hydride platelets with a maximum length of about 50 μm were also present. Radial hydrides near the outside portion were more dominant in Fig. 5(b) and (c) for P3 and P4 specimens. Many radial hydrides precipitated over the outside portion. At the same time, hydrides with circumferential orientation were still found in the area about a third of the wall thickness from the outside.

As explained in Fig. 3, transverse and longitudinal cross-section metallography was done step-by-step on D8/C6-5 and D8/F3-5 segments, respectively. The depth polished in every view step is tabulated in Table 2.

Table 1
Summary of failed segment rods

Rod no.	Segment ID	Irradiation duration	Burnup (GWd/t)	Ramp sequence	Maximum power (kW/m)	Time to failure (min)
P1	D3/F3-3	3 cycles	43.4	Single step	61.4	9
P2	D4/F3-5	4 cycles	56.3	Single step	55.1	149
P3	D8/C6-5	5 cycles	61.1	Single step	42.1	100
P4	D8/F3-5	5 cycles	61.1	Single step	42.8	68
P5	D8/C6-6	5 cycles	60.8	Stair case	44.6	22

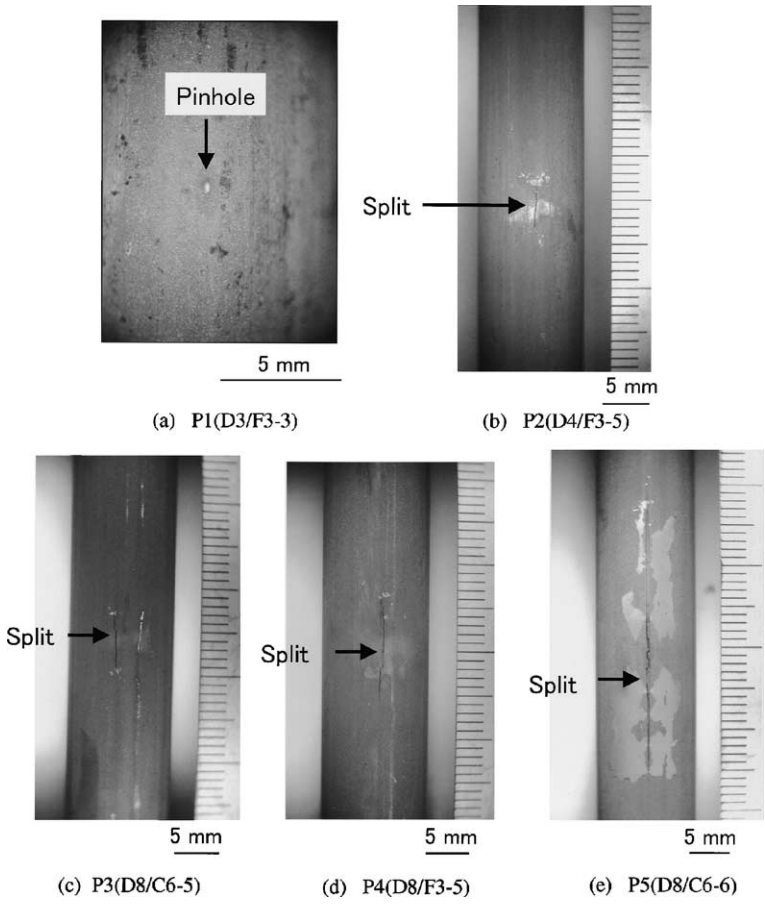

Fig. 1. Visual outside appearances of failed segment rods.

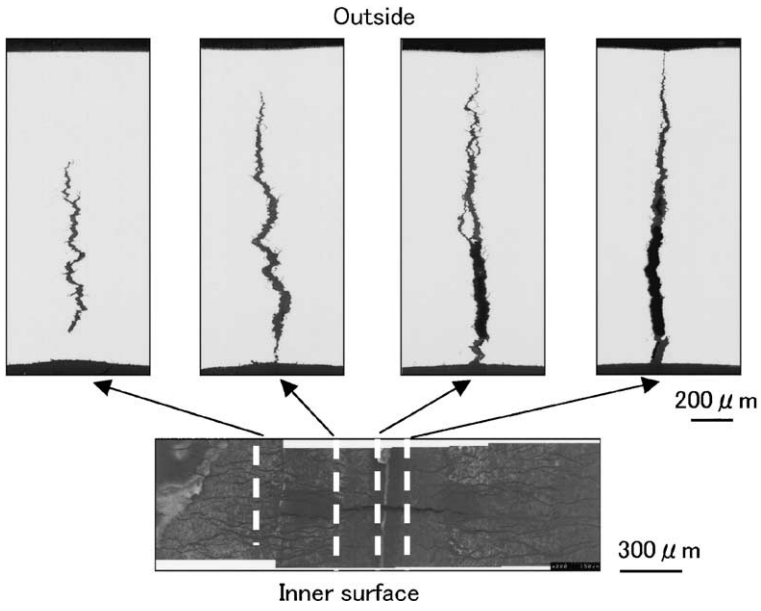

Fig. 2. Transverse views and inner surface of P1(D3/F3-3) segment rod.

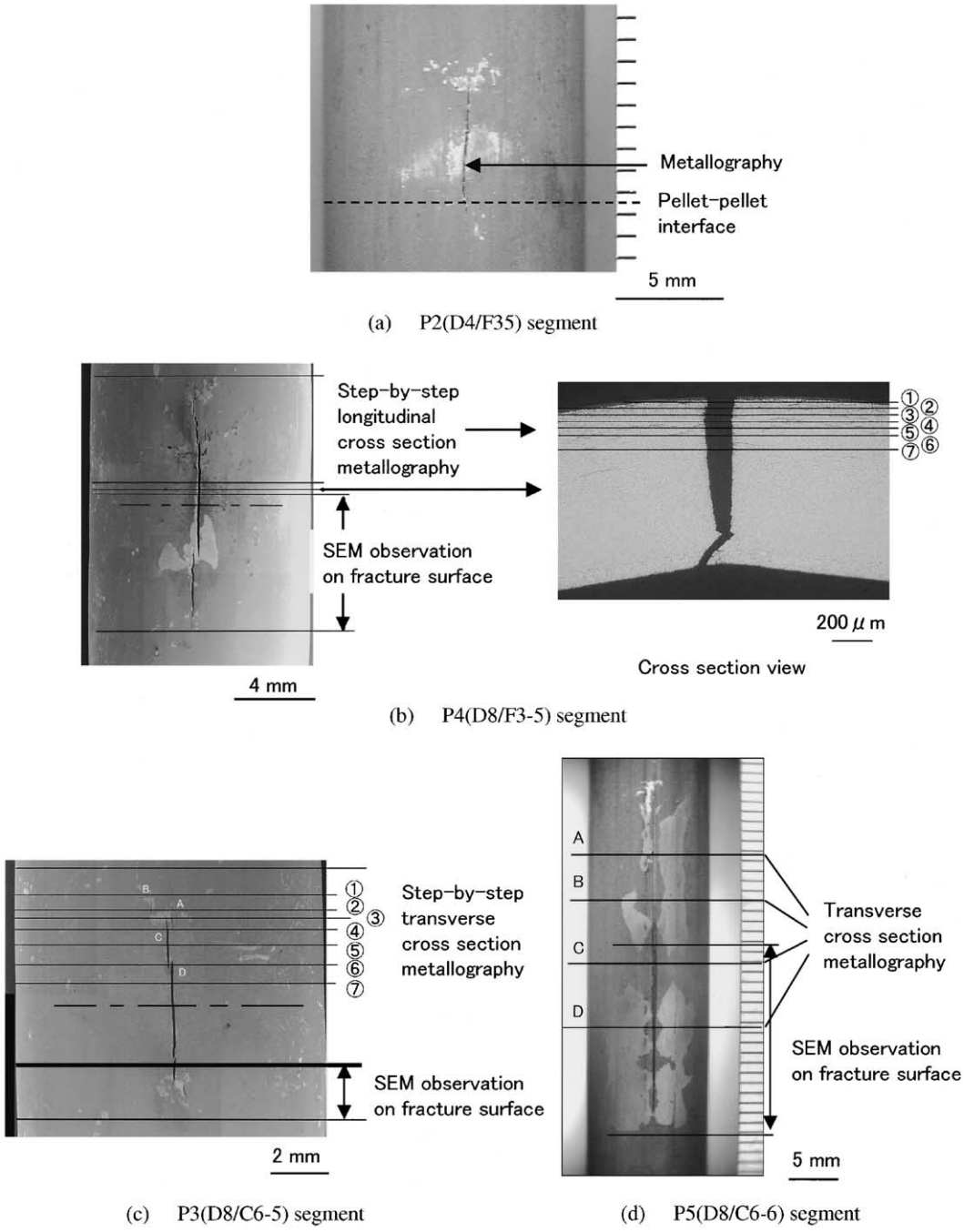

Fig. 3. PIE schemes for failed segment rods with splits.

Transverse views at every step are depicted in Fig. 6. In the view step 1, two incipient cracks appeared and lengthened in views 2 and 3. Another crack C appeared in the view step 3 which grew and finally penetrated the cladding in the step 5. Although two cracks, C and D, were separate on the outer surface as shown in the step 6, they had become one by the step 7. These photographs also revealed that at the sections where the crack penetrated the cladding wall, the crack mainly proceeded in the radial direction and there was significant ductility at the Zr- layer or Zr-layer and the narrow Zry-2 portion just adjacent to the layer. Since it was

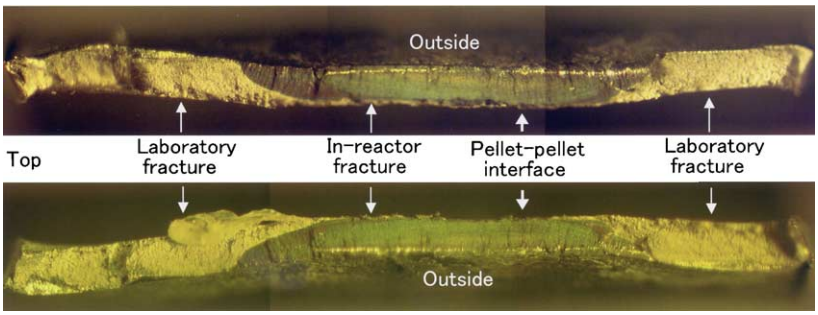

Fig. 4. Fracture surface pair of P2(D4/F3-5) cladding tube.

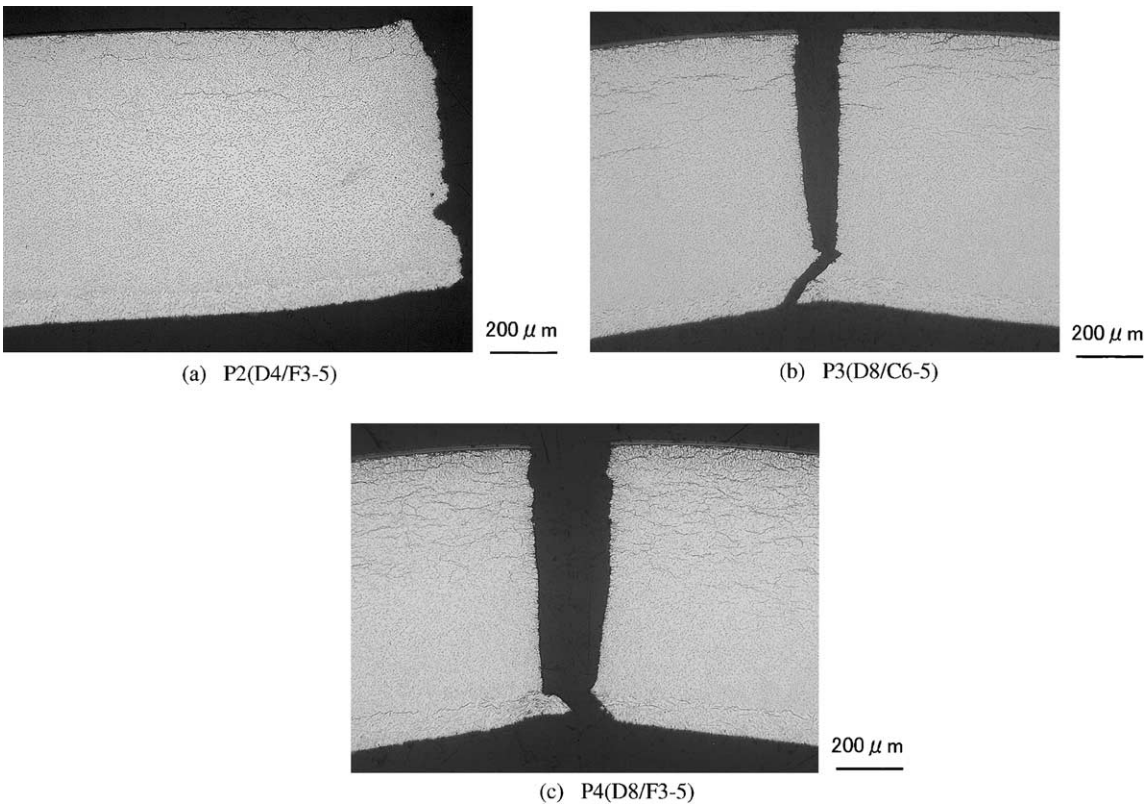

Fig. 5. Transverse views showing hydride distributions and fracture regions for P2(D4/F3-5), P3(D8/C6-5) and P4(D8/F3-5) segment rods.

impossible to distinguish the hydrides from the crack on photographs taken from etched specimens, photographs taken from normally polished specimens were utilized for careful examination of hydride precipitation at the crack tip. A photograph of incipient crack C (in the view step 3) in a normally polished specimen was magnified and image-processed in order to distinguish the crack from hydride platelets. The image-processed photograph in Fig. 7 showed that at the crack tip, hydride platelets with partial cracks were present and hydride platelets without cracks precipitated at the bottom of the par-

Table 2
Depth of step-by-step metallography in μm (each step/total)

Transverse section (step 1 = 0 μm)		Longitudinal section (outside = 0 μm)	
View step 1	0/0	View step 1	30/30
View step 2	550/550	View step 2	30/60
View step 3	330/880	View step 3	30/90
View step 4	500/1380	View step 4	30/120
View step 5	700/2080	View step 5	30/150
View step 6	600/2680	View step 6	40/190
View step 7	550/3230	View step 7	70/260

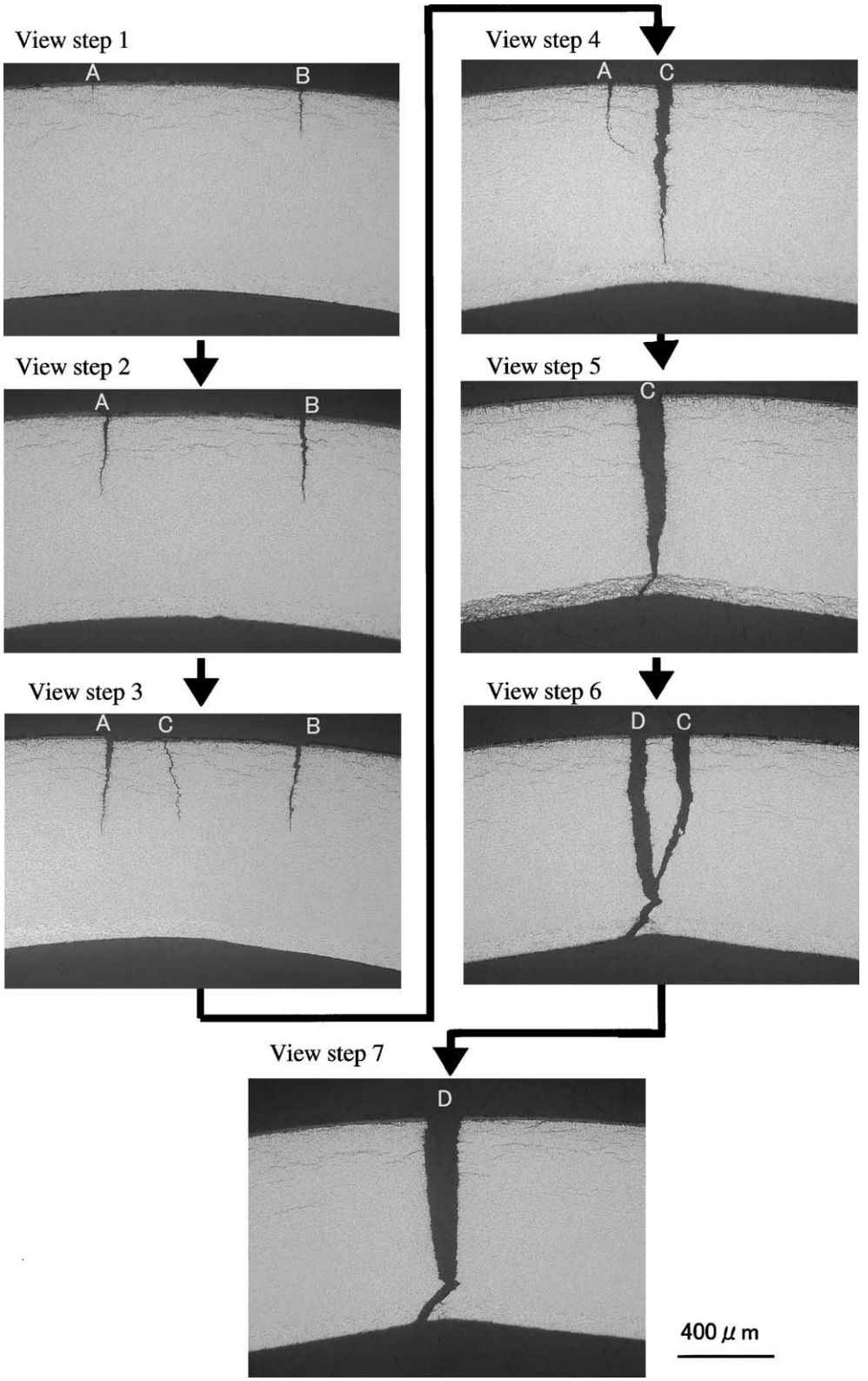

Fig. 6. Transverse views of step-by-step crack morphology in P3(D8/C6-5) specimen.

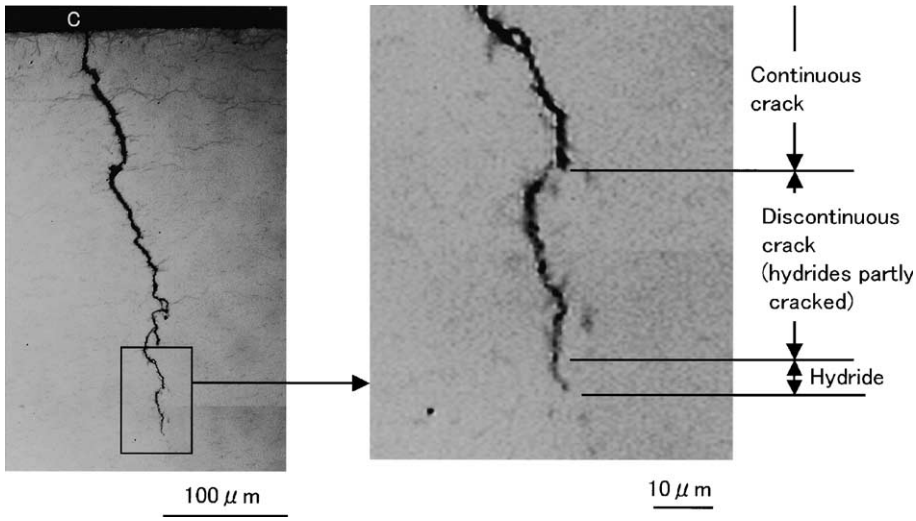

Fig. 7. Detailed morphology of hydrides near crack tip in the transverse view step 3 in Fig. 6.

tially cracked hydrides. The image also showed that there were few hydrides platelets around the crack, except the crack front. Longitudinal views for every step in the P4 specimen are shown in Fig. 8. An interesting hydride distribution at the crack tip was observed in the view step 5, 150 μm from the outside, as shown in Fig. 9. Hydrides platelets distributed around the crack tip, surrounding it. This distribution might be caused by stress distribution around the crack tip. Some incipient cracks in the view step 6 of Fig. 8, 190 μm from the outside, were investigated by the image process method and illustrated in Fig. 10, which shows that the hydrides precipitated at the crack front and they partly cracked also in the longitudinal cross-section.

Since P5 segment rod failed with a comparatively long axial crack, four transverse sections were examined. The optical photographs in Fig. 11 revealed that the crack propagated in the radial direction about 100 μm from outside and was followed by ductile fracture in the upper half, while, in lower the half, just like P2, P3 and P4 rods, the radial crack was predominant and ductility was retained just near the inner surface.

3.3. SEM observation

The outer and inner surfaces, and fracture surface of P2 segment rod are shown in Fig. 12. The outer surface exhibited a noticeable axial crack 'split', but only many tiny cracks appeared on the inner surface. The SEM image of the inner surface indicated that the axial crack was located near a pellet–pellet interface. Fracture surface morphology of the P4 specimens is shown in Fig. 13. Pair fracture surfaces were examined for P3 to confirm the fracture morphology (Fig. 14). Three pairs of matching fracture surfaces are compared in Fig. 15, the first pair shows the surfaces near the outside, the second, about 120 μm from the outside, and the third, about 450 μm from the outside. Comparison of the two matching fracture surfaces in each pair indicated that on a macroscopic level there was an almost perfect fit between the two sides of the crack. A 'hill (H)' on one fracture surface always corresponded to a 'valley (V)' on the matching fracture surface. The morphology of the fracture surface on P5 is shown in Fig. 16.

4. Discussion

Optical photographs on specimens mounted transverse to the tube axis indicate that the most noticeable feature of hydride morphology in cladding tubes from ramp-tested segment rods is the existence of many radial hydrides near the outside as typically shown in Fig. 11(c). Since no radial hydrides such as observed in ramp-tested tubes are found in the claddings that experienced just base exposure (Fig. 17), it is deduced that the radial hydrides near the outside precipitated during ramp tests. Since ramp tests usually cause steep temperature gradients along the tube wall, hydrides that precipitated inside the tube before the ramp test would re-dissolve and diffuse to the outside portion, and then would re-precipitate at the outside portion at relatively lower temperatures. At the same time, hoop stress caused by pellet cladding mechanical interaction (PCMI) could help hydrides precipitate along a radial orientation [9–11]. It has been reported that radial hydrides relatively crack easily under hoop stress, especially under multi-axial stress conditions [12]. That report also notes that the radial hydride length is the most critical factor for fracture behavior. Thus, among the radial hydrides that

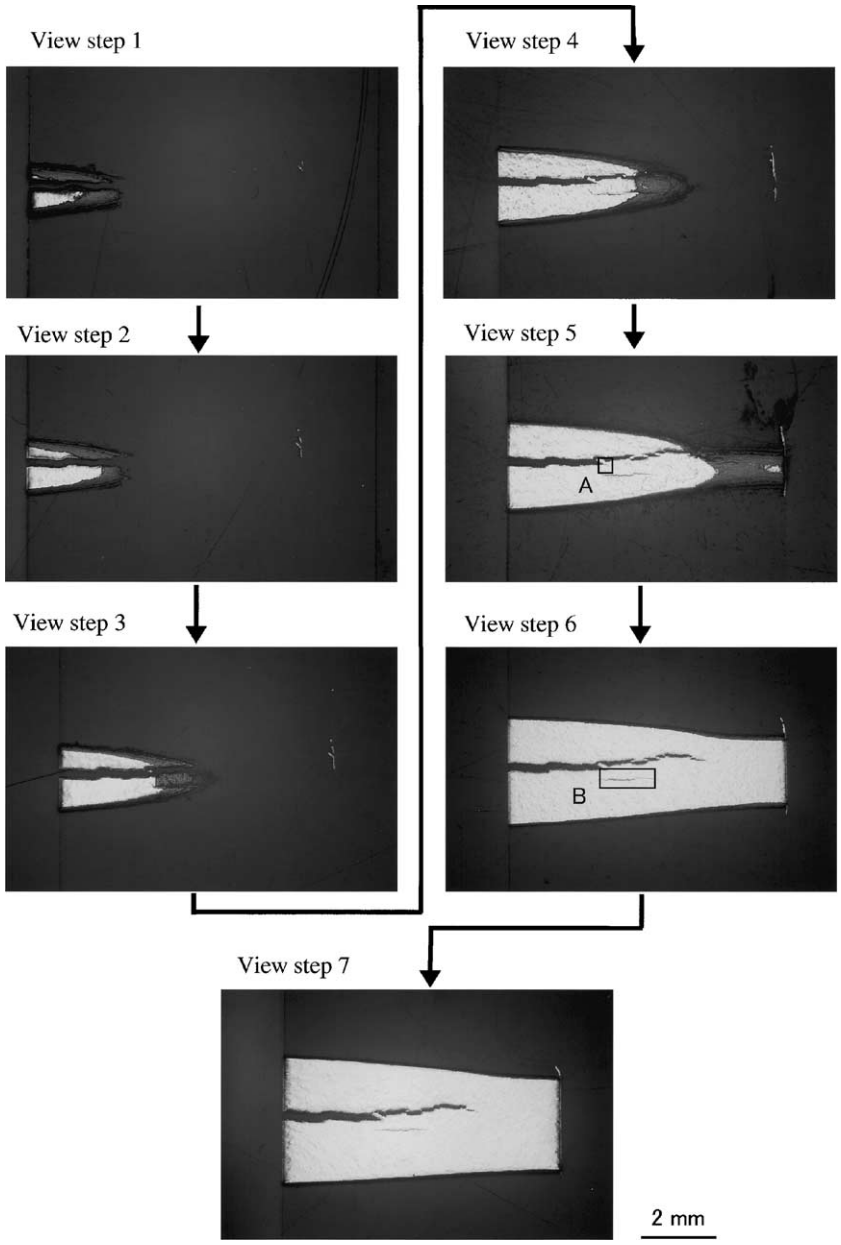

Fig. 8. Longitudinal views of step-by-step crack morphology in P4(D8/F3-5) specimen.

precipitated at the outside portion during the ramp test, a relatively long hydride platelet would crack due to the strain caused by PCMI and cracking of the hydride platelet in the outside portion would initiate an outside-in crack, or segment rod failure.

When the numbers of radial hydride platelet in the cladding outside at pellet–pellet interface and at mid-pellet portion are compared, more hydrides can be seen at the former as shown in Fig. 11. These relatively many radial hydrides at the outside corresponding to pellet–pellet interface portion might be caused by higher hydride concentration in the Zr-layer at pellet–pellet interface than at mid-pellet, as illustrated in Fig. 18. The high hydride concentration in the Zr-layer at pellet–pellet interface is observed in specimens of post-ramp tubes as well as pre-ramp ones. This hydride localization in the Zr-layer at pellet–pellet interface could be induced by slightly lower operating temperatures than those of the bulk of the cladding. Since hydrides in the Zr-layer would act as a hydrogen supplier for radial hydrides at

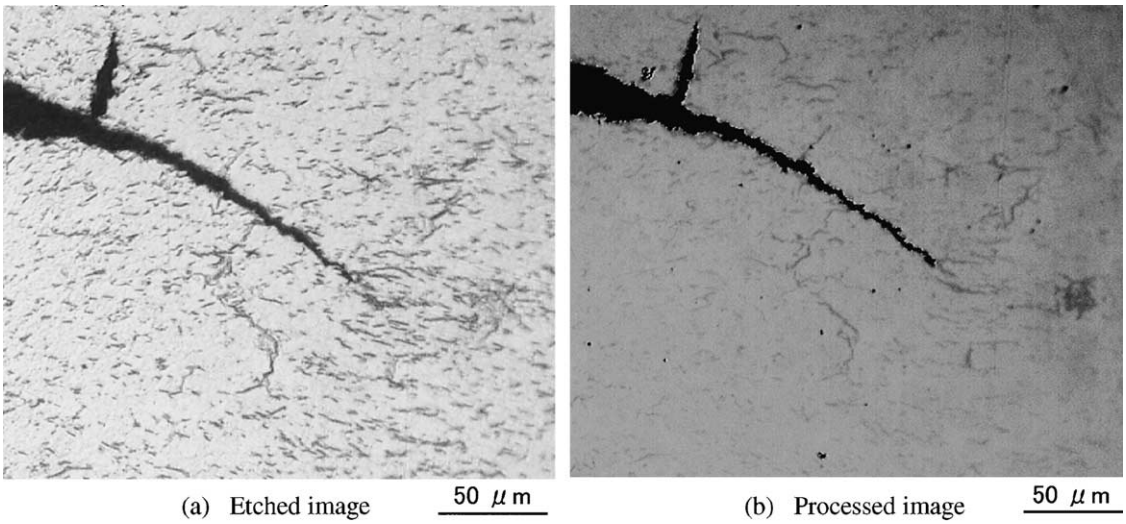

Fig. 9. Detailed morphology of hydrides near crack tip(A) in the longitudinal view step 5 in Fig. 8.

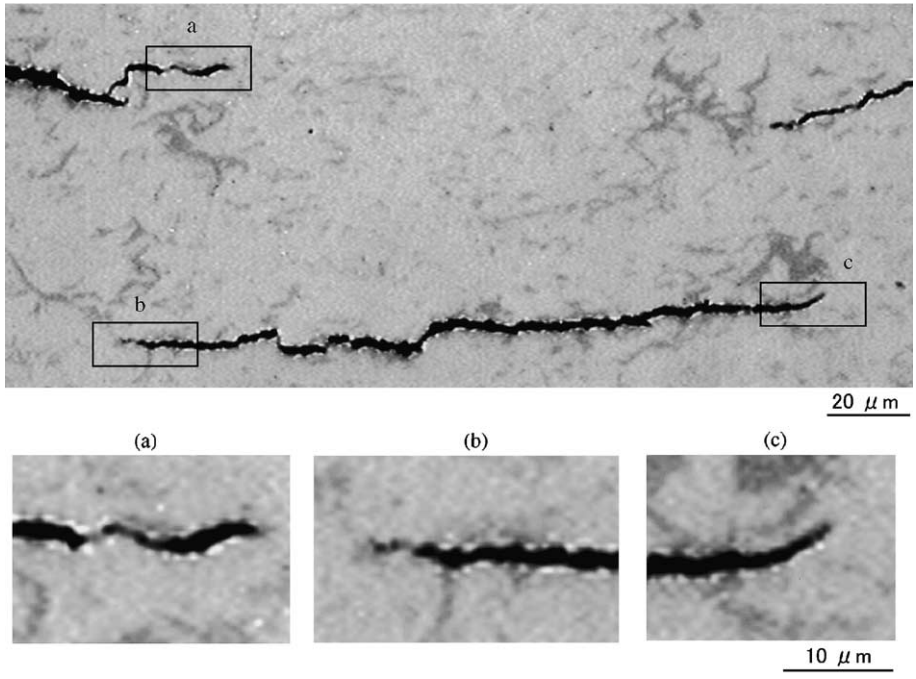

Fig. 10. Detailed morphology of hydrides near crack tip(B) in the longitudinal view step 6 (Fig. 8).

cladding outside during ramp tests, the hydride localization in the Zr-layer might contribute to formation of radial hydride platelets outside at the pellet–pellet interface. These observations suggest that the environment outside at pellet–pellet interfaces could be more critical for crack initiation because of both higher PCMI and higher radial hydride platelet concentration than at the mid-pellet portion. This suggestion would explain why all outside-in cracks penetrated near pellet–pellet interfaces.

Optical photographs from step-by-step observations reveal some interesting hydride behavior at crack tips. A

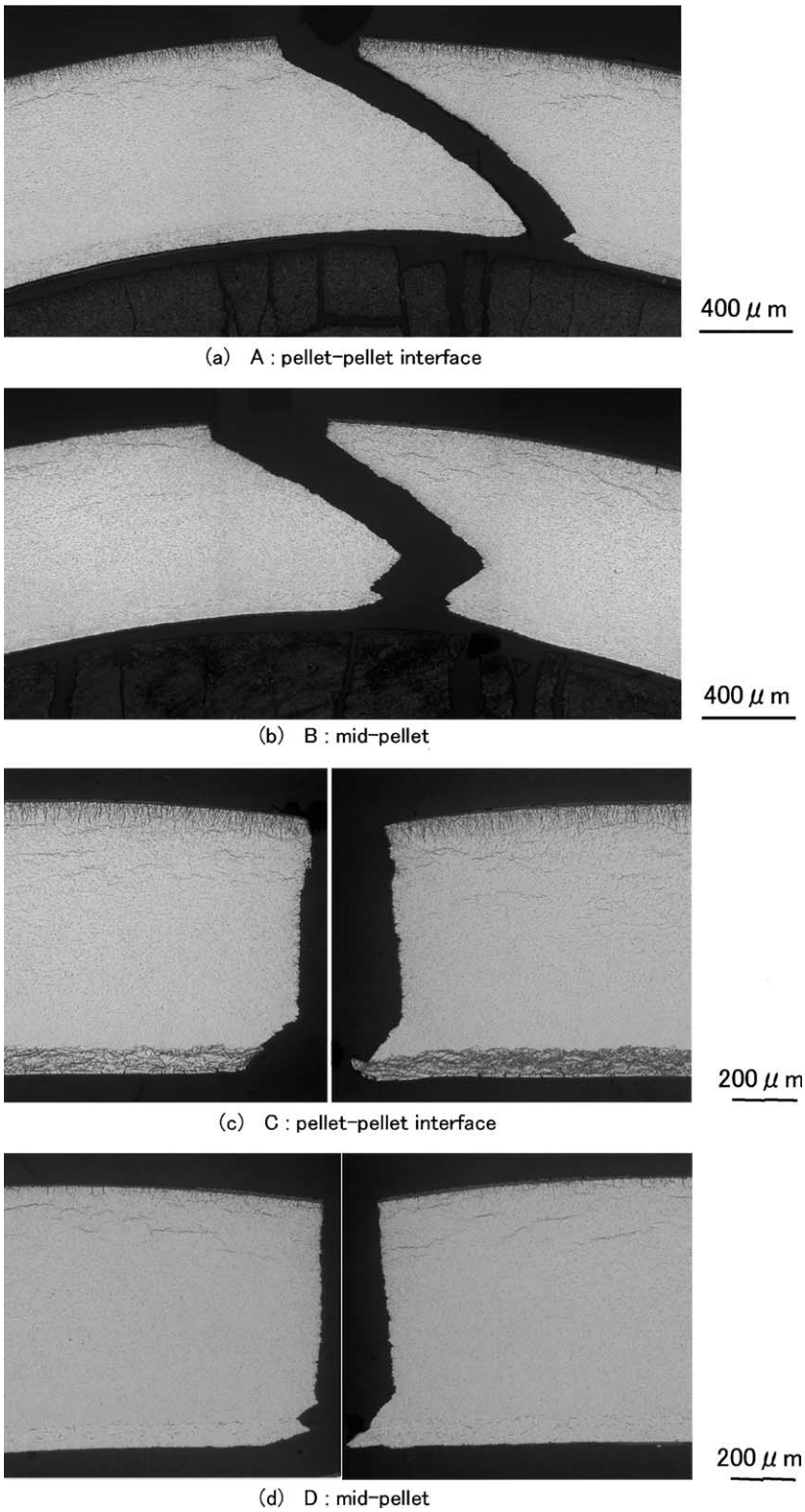

Fig. 11. Transverse views showing hydride distributions and fracture regions for D8/C6-6) segment rod A, B, C and D indicate the transverse sections in Fig. 3(d).

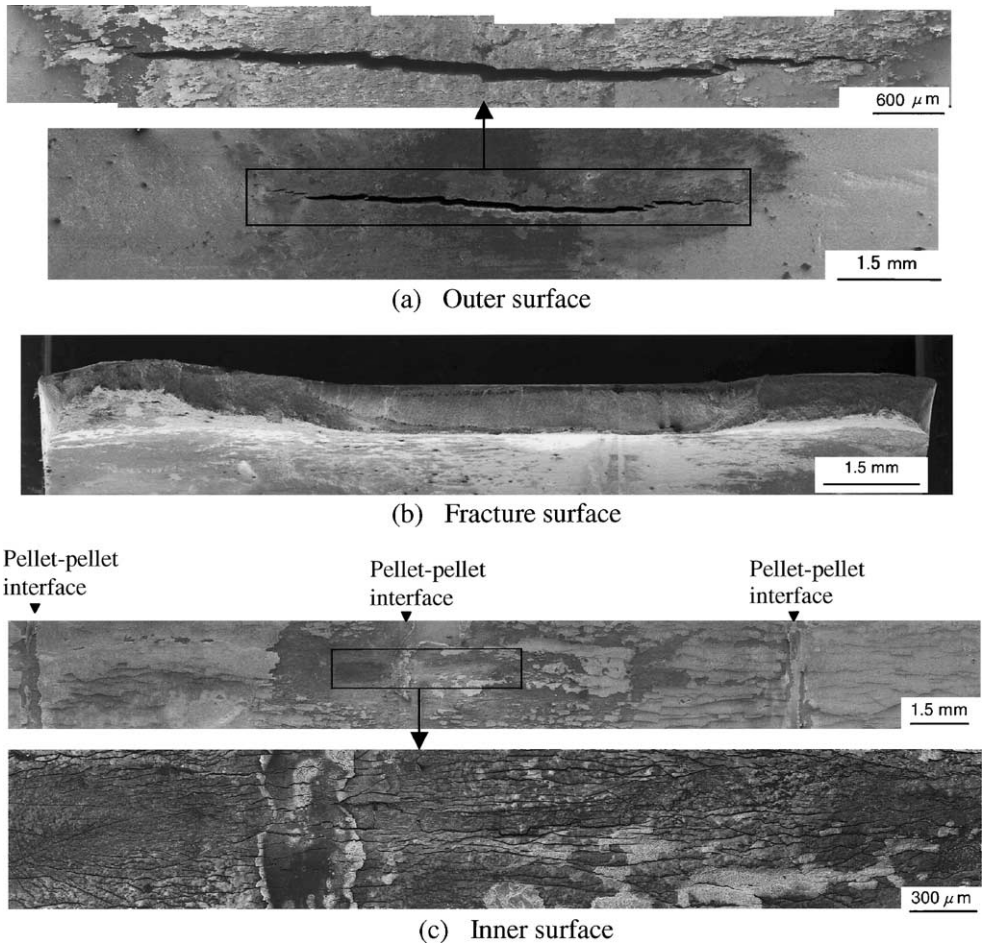

Fig. 12. Overview images of outer, fracture and inner surfaces of crack in P2(D4/F3-5) segment rod.

view of the tip for a comparatively shallow crack shows hydrides surrounding the crack as well as hydrides precipitated at the crack front (Fig. 9). The surrounding hydride distribution might reflect the stress field around the crack tip. However, when cracks advance and the crack tip is located where no hydrides might precipitate under ramp test conditions, as shown in Figs. 7 and 10, just the hydrides that precipitates at the front along the crack orientation are observed. Those hydride platelets are about 2 μm wide in general. Sometimes, the hydrides at the front are followed by partially cracked hydrides (Fig. 7). These observations suggest that the crack would propagate through the cracking of hydrides that precipitate at the crack tip. Detailed metallographic optical photos, thus, reveal that hydrides are responsible for the outside-in crack propagation.

Although stripe patterns are visible on the fracture surface of the P2 specimen when observed with the periscope, such patterns are not recognized on SEM images. This result suggests that the patterns might be originated from a change in oxide thickness on the surface. It is usually recognized that a very thin oxide film on metals causes an interference color and the color varies with the thickness [13]. The fact that SEM images of fracture surfaces are almost clear and do not show any oxidized features on them seems to support the above idea.

Morphology of the fracture surfaces of P2, P3, P4 and P5 specimens observed by a SEM shows the same appearance. Overall, the surfaces are rather smooth. As Figs. 13 and 16 indicate, the surfaces near the outside are most brittle and the area deeper than about 50–100 μm shows randomly tangled white lines that are, at a glance, similar to elongated shallow dimples. However, careful SEM observations on two opposing fracture surfaces of the P3 specimens (Fig. 15) reveal that the fracture surfaces are essentially brittle in all areas. It is deduced that the white lines, which were apparently similar to

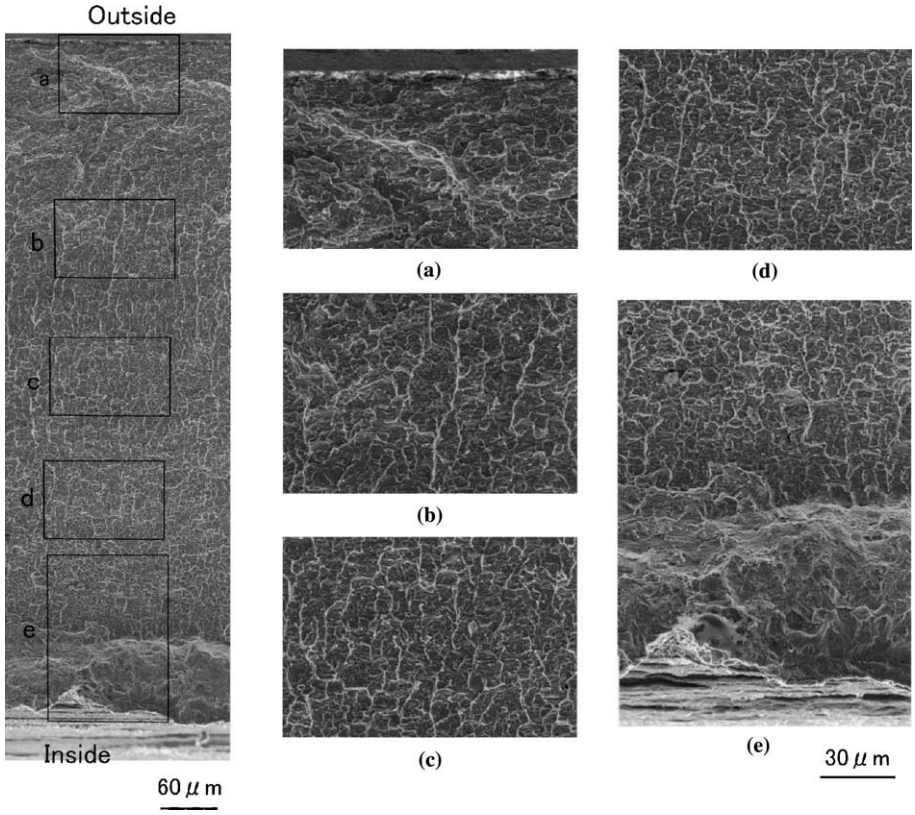

Fig. 13. Morphology of fracture surface of P4(D8/F3-5) specimen.

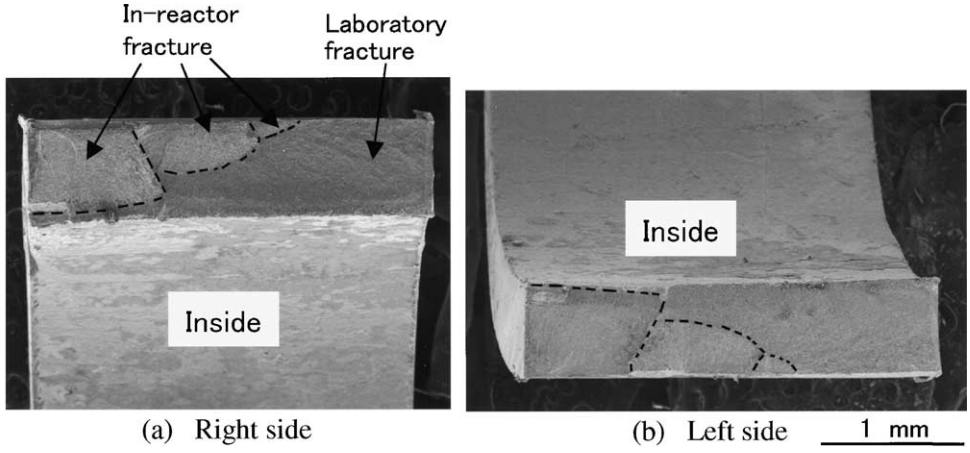

Fig. 14. A pair of P3(D8/C6-5) specimen used for SEM observation.

elongated dimples, might be caused by the connection process of independent small hydride cracks to make a crack. The surfaces are, however, ductile near the inside, or at the Zr-layer.

When optical microscopic and fractographic observations are comprehensively taken into account, a possible crack initiation and propagation process could schematically be summarized as in Fig. 19. The tem-

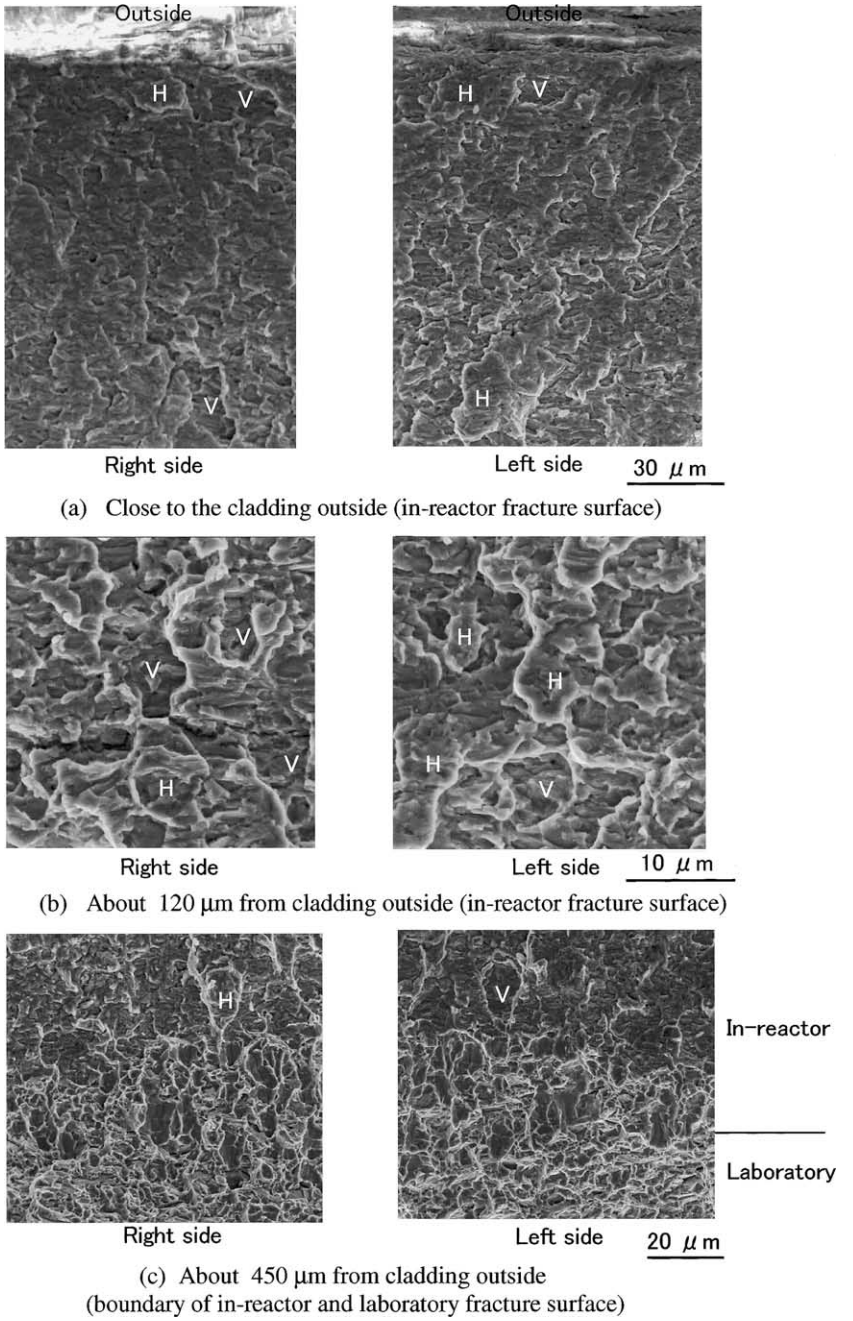

Fig. 15. Three pairs of SEM images of two matching fracture surfaces; H: hill, V: valley.

perature gradient and stress produced by power ramp tests cause radial hydrides to concentrate at cladding outside. Then the fracture of the hydrides due to strain (or stress) by PCMI would trigger the outside-in cracking. Since hydride platelets mechanically fracture at the initiation process, the morphology of the fracture surface is most brittle. In the crack propagation process, hydrides precipitate at the crack front and then grow to a certain length to crack at the tip. By repeating the same process the crack advances and finally, when the residual wall thickness becomes thin enough to be torn mechanically, the cladding fails by a ductile process. Although hydrides in the cladding tube is responsible for the crack initiation, an evaluation of hydrogen content

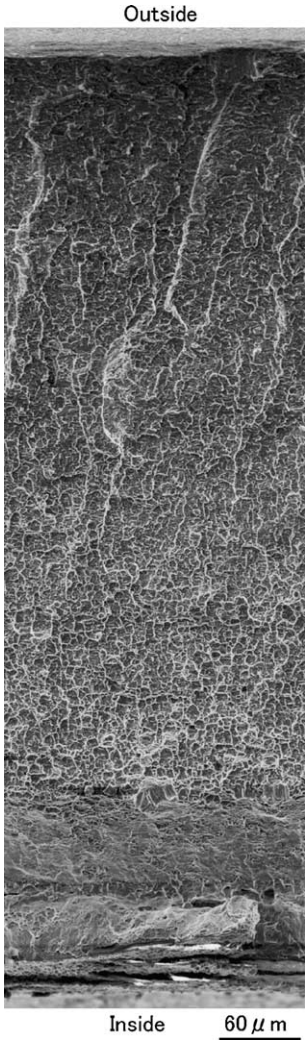

Fig. 16. Morphology of fracture surface on P5(D8/C6-6) specimen.

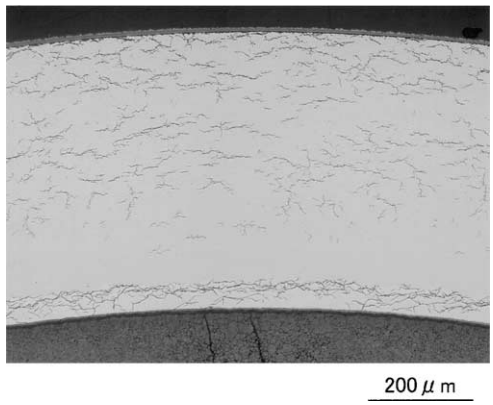

Fig. 17. Typical hydride morphology in the cladding tube of a full length rod cooled down in a BWR after five irradiation cycles.

distribution in the cladding tube suggests that it would be difficult for hydrogen in the tube to take charge of the hydride precipitation at the crack front in most of the propagation region. A hydrogen content profile along the tube wall during a ramp test analyzed by using PIE results is shown in Fig. 20. The initial hydrogen content distribution before ramp test rod was measured by using the metallographic pictures of the claddings that experienced just base exposure (Fig. 17), and the final hydrogen content distribution of the ramp-tested rod, by Fig. 5, for example. Using the measured initial distribution profile, the analysis was conducted so that the final hydrogen content profile fit the measured data. The calculation results are plotted in Fig. 20 as well as measured data profiles. The analysis reveals the hydrogen content is too low for the hydrogen in cladding to precipitate in most of the propagation region at high temperature, even if hydrogen solubility, affected by stress concentration at the crack tip, is taken into ac-

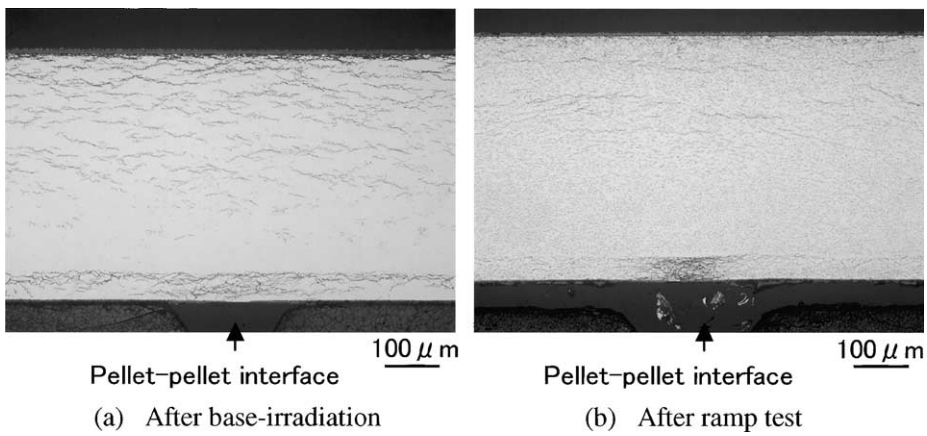

Fig. 18. Longitudinal views showing hydride distributions at pellet–pellet interfaces for segment rod with five irradiation cycles.

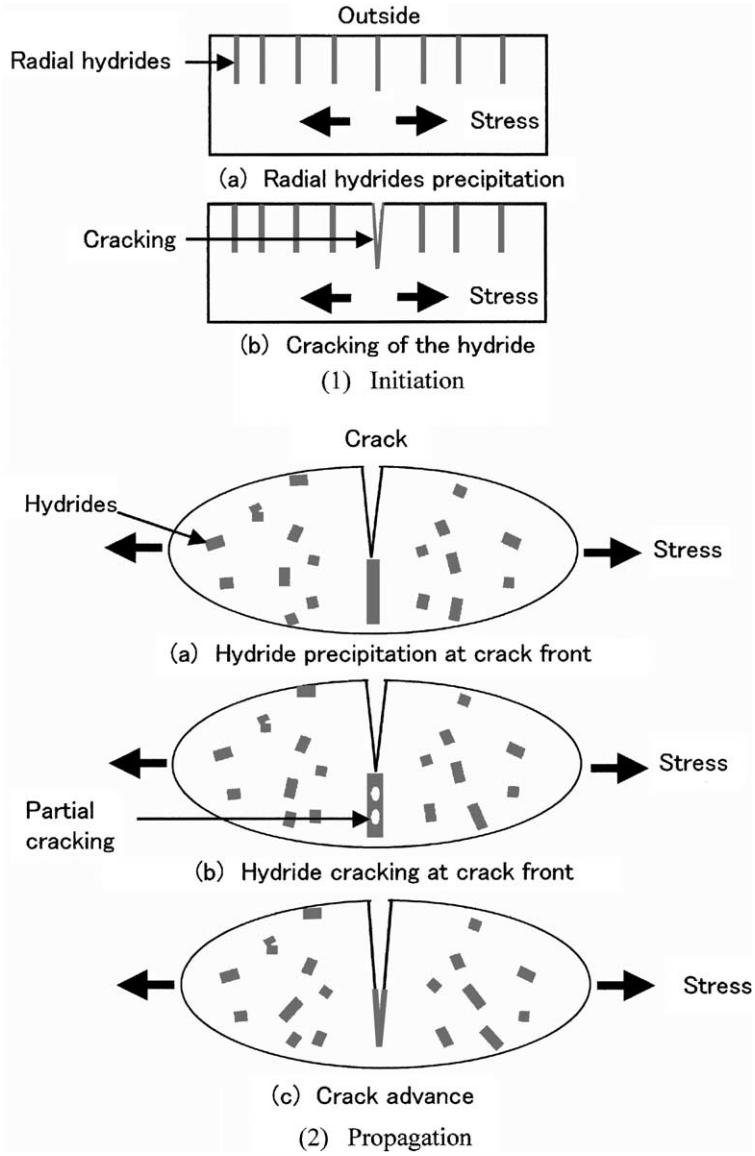

Fig. 19. Schematic of crack initiation and propagation process.

count. Therefore, another mechanism seems to be needed to explain the hydride precipitation at the crack front. One possible idea is the absorption of hydrogen at the fracture surface, especially at the crack front surface. When radial hydrides fracture, coolant goes into the crack and the diffusing steam begins to react with the fracture surfaces. Oxygen is stripped from the steam by the simplified reactions below:

$$2H_2O + Zr \rightarrow ZrO_2 + 2H_2$$

When the gas mixture becomes sufficiently enriched in hydrogen, absorption will occur by breaking down the protective oxide on the fracture surfaces. A simple calculation reveals that only a few nano-meters of oxide thickness would be good enough for the steam to be completely changes to hydrogen gas, because the crack width is so narrow, about 10 μm or less. This result indicates that the crack would be filled with hydrogen in comparatively short time after steam invasion. Since the steam changes to the same number of moles of hydrogen gas, the crack would be filled with almost pure hydrogen of about 7 MPa, the coolant pressure of the ramp test. After the steam changes to hydrogen, since the crack is very narrow and deep, hardly any new coolant steam would come into the cracking space to degrade the hydrogen purity. Thus, once the crack was filled with

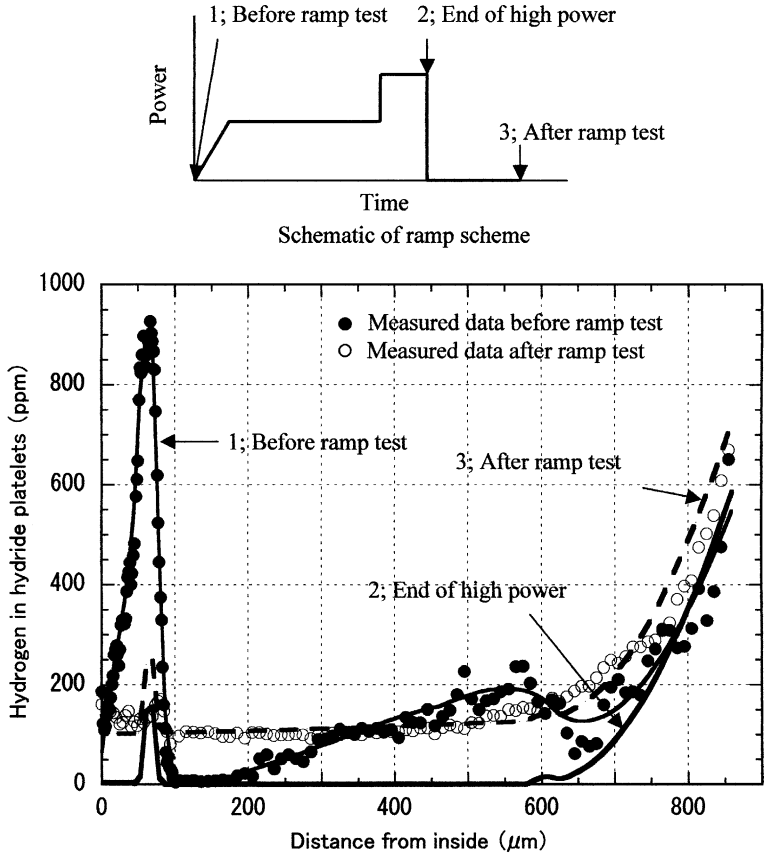

Fig. 20. Calculated hydride profiles along radial direction during ramp test (Average hydrogen content: 180 ppm).

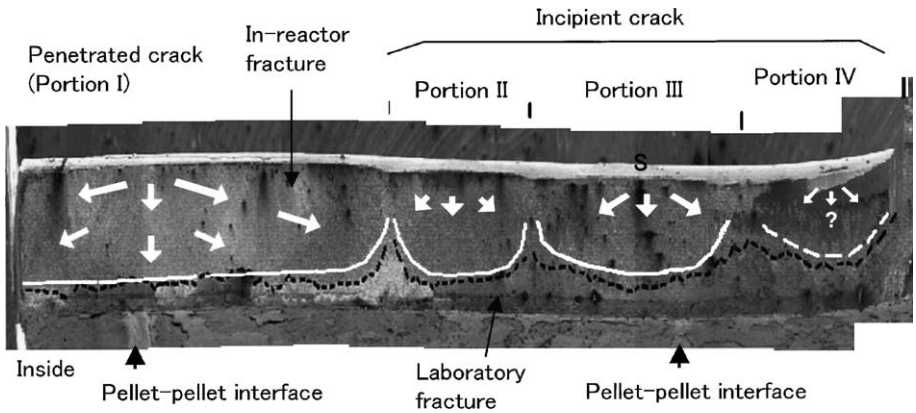

Fig. 21. Schematic of crack propagation scheme for P5(D8/C6-6) specimen analyzed by chevron patterns. The observed area is 'SEM observation on fracture surface' in Fig. 3(d). Black dotted lines denote the boundary of brittle and ductile fracture surfaces. White lines approximately show the outlines of four portions of in-reactor fracture surfaces.

hydrogen, the crack would propagate by a hydrogen gas cracking (HGC) mechanism [14–16]. When some amount of hydrogen is absorbed through the fracture surface and new steam flows into the crack, since the crack tip is located at the bottom, hardly any new steam would reach the bottom and almost pure hydrogen atmosphere would be maintained there. Furthermore, the hydride fracture at the crack front exposes a new metal surface at the front, which would promote hydrogen absorption there, leading to hydride precipi-

tation and again, hydride cracking. By repetition of hydrogen absorption, precipitation and cracking, the crack would advance to farther towards the inside and finally, when only a thin residual wall remains, it would penetrate the cladding in ductile fracture.

The relatively long axial split on the P5 segment rod might be attributed to the ramp test scheme. The rod is exposed to a stair mode ramp test. That means there is a possibility that one more step power rise might be added while outside-in cracking is in progress. The extra power rise might advance the crack in both inside and axial directions, which would cause comparatively shorter time to failure (Table 1) and longer axial split (Fig. 1(e)) than those of other segment rods, P2, P3 and P4. Chevron patterns on the fracture surfaces of P5 are utilized to analyze the direction of crack propagation [6,7]. The result is schematically shown in Fig. 21, which suggests that fracture surface could be classified to four areas indicated Portions I, II, III and IV as illustrated in the Fig. 21. This figure indicates that the crack penetrates at Portion I and at other three portions, II, II and IV, it does not. The direction of crack propagation analyzed by chevron patterns on each portion is designated by white arrows. For example, the arrows show that the crack in portion III started at outside point S in Fig. 21 and propagated to both axial sides and connected with portions II and IV, finally making a long axial split.

5. Conclusion

Careful examinations of segment rods which failed by ramp tests after four and five cycles of base-irradiation show that hydride cracking is responsible for the failure mechanism. For crack initiation, hydrogen behavior caused by power ramp test is essential. The temperature gradient along the cladding wall and stress due to the ramp test precipitate radial hydrides on the tube outside. Then, the hydride fractures because of hoop strain or stress by PCMI, that is, the initiation of outside-in cracking. Since hydrogen that originally included in the cladding plays a main role, the mechanism is somewhat similar to that of secondary degradation failure, or delayed hydride cracking (DHC). However, in the crack propagation process, it was deduced that, although hydride cracking at the crack front was fundamental to the process, hydrogen absorbed at the crack tip might be a prerequisite for the hydride formation. Therefore, the mechanism of outside-in cracking observed in power ramp tests would be different from that of the usual secondary degradation mechanism in which hydrogen in cladding tubes was responsible for crack propagation. The ramp test results suggest that hydride orientation would play a critical role for fuel rod behavior as well as hydrogen content. In order to assess the fuel rod behavior at high burnups, better understanding of the dissolution, diffusion and local precipitation of hydrogen in cladding tubes in operation must come from future work.

Acknowledgements

This study was carried out mainly under the direction of committees of NUPEC. The authors gratefully acknowledge the helpful comments and encouragement of the late Professor Emeritus Tadatsune Okubo (Sophia University) on the discussion. The authors also greatly acknowledge the Ministry of Economy, Trade and Industry (METI) for the sponsorship on this study.

References

[1] H. Ohara et al., in: Proceedings of the International Topical Meeting on LWR Fuel Performance, ANS, West Palm Beach, Florida, 17–21 April 1994, p. 674.
[2] J.H. Davies et al., Fuel Ramp Tests in Support of a Barrier Fuel Demonstration, GEAP-22076, July, 1984.
[3] B. Cox, J.C. Wood, in: C.S. Tedman Jr. (Ed.), Corrosion Problems in Energy Conversion and Generation, Electrochemical Society, New York, 1974.
[4] J.H. Davies, G.A. Potts, in: Proceedings of the International Topical Meeting on LWR Fuel Performance, ANS, Avignon, France, 21–24 April 1991, p. 272.
[5] L. Jonsson, B. Grapengiesser, G. Lysell, in: Proceedings of the International Topical Meeting on LWR Fuel Performance, ANS, Avignon, France, 21–24 April 1991, p. 371.
[6] K. Edsinger, in: Proceedings of the International Topical Meeting on LWR Fuel Performance, ANS, Park City, Utah, 10–13 April 2000, p. 162.
[7] G. Lysell, V. Grigorev, P. Efsing, in: Proceedings of the International Topical Meeting on LWR Fuel Performance, ANS, Park City, Utah, 10–13 April 2000, p. 216.
[8] H. Sakurai, Y. Wakashima, K. Ito, M. Sasaki, T. Nomata, Y. Tsukuda, H. Hayashi, O. Kubota, in: Proceedings of the International Topical Meeting on LWR Fuel Performance, ANS, Park City, Utah, 10–13 April 2000, p. 515.
[9] M. Leger, A. Donner, Can. Metall. Q. 24 (1985) 235.
[10] H. Stehle, W. Kaden, R. Manzel, Nucl. Eng. Des. 33 (1975) 155.
[11] D. Hardie, M.W. Shanahan, J. Nucl. Mater. 55 (1975) 1.
[12] M.P. Puls, Metall. Trans. A 19A (1988) 1507.
[13] A.T. Fromhold, Jr., Theory of Metal Oxidation, Vol. 1 – Fundamentals, North-Holland, 1976 (Chapter 1).
[14] C.E. Coleman, B. Cox, ASTM STP 824 (1984) 675.
[15] R.G. Rowe, Scr. Mater. 38 (1998) 1495.
[16] R.G. Rowe, Scr. Mater. 40 (1998) 249.
[17] The Annual Report on Irradiation Tests of High Burnup Fuels in Fy 2001, in: Integrated Evaluation on Irradiation Behavior of BWR High Burnup Fuel, March 2002 (in Japanese).
[18] D. Schrire, G. Lysell, G. Frennning, G. Ronnberg, A. Jonsson, in: Proceedings of the International Topical Meeting on LWR Fuel Performance, ANS, West Palm Beach, Florida, 17–21 April 1994, p. 398.